Double-Resonance Two-Photon Spectroscopy of Hydrogen Molecular Ions for Improved Determination of Fundamental Constants

Florin Lucian Constantin

Double Resonance Two-Photon Spectroscopy of Hydrogen Molecular Ions for Improved Determination of Fundamental Constants

Florin Lucian Constantin

Laboratoire PhLAM, CNRS UMR 8523, 59655 Villeneuve d'Ascq, France

e-mail: FL.Constantin@univ-lille1.fr

Abstract: A spectroscopy scheme is proposed for the detection of the two-photon rotational transition (v,L)=(0,0)→(0,2) and the two-photon rovibrational transition (v,L)=(0,0)→(2,0) of cold trapped HD^+ ions by dissociation. The two-photon lineshapes are calculated using a rate equation model. The resolution is at the 10^{-13} level. The lightshift for selected hyperfine components of the two-photon transitions is evaluated using the two-photon operator formalism. The experimental accuracy with two-photon transitions of trapped HD^+ ions is estimated at the 10^{-12} level, which corresponds also to the accuracy of the theoretical calculations. The comparison of experimental data and theoretical calculations for HD^+ and H_2^+ transitions may lead to an independent determination of the Rydberg constant, the proton-to-electron mass ratio and the deuteron-to-proton mass ratio. It may provide a measurement of the proton and deuteron radii by molecular spectroscopy. Depending on possible issues of the proton radius puzzle in atomic spectroscopy, two-photon spectroscopy of hydrogen molecular ions may lead to an improvement of the determination of the proton-to-electron mass ratio and deuteron-to-proton mass ratio at the 10^{-12} level.

Keywords: Two-photon spectroscopy; two-photon lightshift; cold trapped ions; proton-to-electron mass ratio; deuteron-to-proton mass ratio; proton and deuteron radii

I. INTRODUCTION

The hydrogen molecular ions (HMI) have simple three-body structure that is well suited for testing molecular quantum mechanics. *Ab-initio* calculations of their energy levels in the ground electronic state were performed with high accuracy. The strategy was to use variational wavefunctions and to take into account quantum electrodynamics (QED) higher order corrections to the non-relativistic energies of the rovibrational levels. The fundamental rovibrational frequencies were calculated with an uncertainty of 7.6×10^{-12} [1-6]. Doppler-limited spectroscopy was performed on HMI maintained in radiofrequency traps and sympathetically cooled by laser-cooled Be^+ ions. State-selective detection of HMI transitions may be provided by resonance-enhanced multiphoton dissociation (REMPD). Since 2007, measurements of different dipole-allowed E1 rovibrational transitions on cold trapped HD^+ ions were performed [7-9]. The experimental uncertainty with infrared transitions was improved at 1.1×10^{-9} [9]. The agreement between experimental results and theoretical calculations, within an uncertainty of 1.1×10^{-9} [9], allowed a test of the QED, a determination of the proton-to-electron mass ratio and a constraint of the effect of fifth forces in molecular spectroscopy [10]. Doppler-free spectroscopy may lead to an improvement of the accuracy. Two-photon spectroscopy of HD^+ ions was suggested in [11,12]. Terahertz spectroscopy of cold trapped HD^+ ions in the Lamb-Dicke regime, demonstrated recently [13], allowed Doppler-free resolution at the kHz level with an uncertainty of 3×10^{-10}. The improved accuracy of the electron mass in CODATA 2014 [14] motivated a recalculation of the HD^+ energy levels and a determination of the proton-to-electron mass ratio at 2.5×10^{-9} [15].

This contribution discusses an approach to measure conjointly two-photon rotational and rovibrational transitions of HD^+, that was suggested in [12]. Precisely, the scheme with cold trapped HD^+ ions that was presented in [16] is extended here to probe the E1-E1 rotational transition (v,L)=(0,0)→(0,2) and the E1-E1 rovibrational transition (v,L)=(0,0)→(2,0) with a detection based on the photodissociation of the (v,L)=(2,0) level. The main motivation for this approach is to benefit of Doppler-free resolution for both transitions. In addition, the sensitivity of the HD^+ ion energy levels of the ground vibrational state to static electric fields [17] or magnetic fields [18] decreases in general with L. The two-photon transition (v,L)=(0,0)→(0,2) may provide smaller systematic frequency shifts than the one-photon transition (v,L)=(0,0)→(0,1) probed in the Lamb-Dicke regime. Moreover, the hyperfine structure is simpler for states with L=0 [19]. The most intense coupling between L=0 states of HD^+ with two photons of equal frequency is between the v=0 and v=2 vibrational levels [20]. The two-photon transition rates and the

lightshifts are calculated using the two-photon operator formalism [21]. Blackbody radiation (BBR) at room temperature drives transitions between rotational energy levels in the ground vibrational state of the HD^+ ions. The two-photon lineshapes are calculated using a set of coupled rate equations of the populations in the energy levels addressed by these transitions. The Zeeman shifts and the lightshifts are estimated. Finally, it should be noted that the rovibrational energy levels of the HMI are described with a two-body effective hamiltonian depending on the reduced mass of the nuclei [22]. The comparison of theoretical calculations with experimental frequencies for transitions of HD^+ ion may provide determination of a nuclear to electron mass ratio, by assuming that the other nuclear to electron mass ratio is known. The determination of both nuclear-to-electron mass ratios would require use of transitions from different HMI. This contribution proposes an approach for determination of fundamental constants that exploits conjointly two-photon rotational and rovibrational transitions of HD^+ and H_2^+.

II. Two-photon Transition Rates, Lineshapes and Lineshifts

A. Hyperfine structure of the energy levels

The energy levels of HD^+ have a hyperfine structure induced by various spin-spin and spin-orbit interactions. The spin coupling scheme is that from [19] :

$$\vec{F} = \vec{S}_e + \vec{I}_p ; \vec{S} = \vec{F} + \vec{I}_d ; \vec{J} = \vec{L} + \vec{S} \tag{1}$$

using the spin operators for the electron $\vec{S}_e$, the proton $\vec{I}_p$, the deuteron $\vec{I}_d$, the rotational angular momentum operator $\vec{L}$, and the total angular momentum operator $\vec{J}$. The hyperfine eigenvectors |v,L,F,S,J> are labelled with the vibrational and the angular momentum quantum numbers. For each rovibrational level, the spin couplings are described with a simplified effective hyperfine Hamiltonian [23] that takes into account the Fermi contact and the magnetic dipolar hyperfine interactions for the proton, deuteron and the spin-rotation interaction :

$$H_{eff} = b_H \vec{I}_p \cdot \vec{S}_e + c_H I_{p,z} \cdot S_{e,z} + b_D \vec{I}_d \cdot \vec{S}_e + c_D I_{d,z} \cdot S_{e,z} + \gamma \vec{S} \cdot \vec{L} \tag{2}$$

The parameters b_H, c_H and γ are taken from [19] and b_D, c_D are estimated with the values of the proton and deuteron gyromagnetic factor given by CODATA 2014 [14]. The effective hyperfine Hamiltonian is diagonalized for each rovibrational level, leading to the hyperfine energies $\Delta E^{v,L,n}$

and the mixing coefficients $\beta_{F,S}^{v,L,n}$. The eigenvectors |v,L,n> of the mixed basis are labelled with an integer n and expressed as a linear combination of the pure basis eigenvectors :

$$\left|v,L,n\right\rangle = \sum_{F,S} \beta_{F,S}^{v,L,n} \left|v,L,F,S,J\right\rangle \tag{3}$$

The |v,L,n> level is labelled with the |v,L,F,S,J> quantum numbers associated to the $\beta_{F,S}^{v,L,n}$ coefficient with the highest absolute value. The hyperfine structure of HD^+ ion energy levels probed by the double resonance spectroscopy scheme is shown in Figure 1.

In presence of a magnetic field, the hyperfine levels are split into sublevels $|v,L,n,J_z>$ labelled by the quantum number J_z of the projection of the total angular momentum on the field axis. The Zeeman Hamiltonian was diagonalized and the energies of the sublevels were approximated with a quadratic dependence on the magnetic field [18].

B. Two-photon transition rates

Two-photon excitation of trapped HD^+ ions is performed using the interaction with two counterpropagating waves with equal pulsation ω, electric field amplitudes $E_{01,02}$ and polarisation states $\vec{\varepsilon}_{1,2}$. The waves are tuned near the two-photon resonance at $\omega_{ge}/2$ such as the relaxation rates and the Doppler shifts are smaller than the detuning to the intermediate energy level $\omega-\omega_{gr}$. The molecular ion-electric field coupling is described in the electric dipole approximation using the two-photon operator formalism [21] :

$$Q^S_{\vec{\varepsilon}_1\vec{\varepsilon}_2} = \frac{Q_{\vec{\varepsilon}_1\vec{\varepsilon}_2} + Q_{\vec{\varepsilon}_2\vec{\varepsilon}_1}}{2}; Q_{\vec{\varepsilon}_i\vec{\varepsilon}_2} = \left(\vec{D}\vec{\varepsilon}_1\right)\frac{1}{\hbar\omega - H_0}\left(\vec{D}\vec{\varepsilon}_2\right) \tag{4}$$

The molecule-fixed dipole operator $\vec{\mu}$ is rotated into the space-fixed system to yield the dipole operator $\vec{D}$ [24]. HD^+ ions are addressed with waves with polarizations chosen between the standard polarisations π, σ^+, σ^-. The two-photon transition operator Q^S_{p1p2} can be expressed in function of the standard components D_{pi} with $p_i=\{-1,0,1\}$. The dipole transition matrix elements between hyperfine states are derived with the spherical tensor formalism using transition dipole moments $\mu_{vL,v'L'}$ calculated in [25].

The two-photon transition probability per unit time is derived using the second-order time-dependent perturbation theory [21] :

$$\Gamma_{ge}^{(2)} = \frac{P_1 P_2}{(S\hbar\varepsilon_0 c)^2} \left| \langle g | Q^S_{\vec{e}_1 \vec{e}_2} | e \rangle \right|^2 \frac{\Gamma_e}{4\delta\omega^2 + \Gamma_e^2/4} \tag{5}$$

in function of the powers of the stationary waves $P_{1,2} = 2\varepsilon_0 S c E_{01,02}^2$ (electric field amplitudes $2E_{01,02}$), the beam area S, the radiative linewidth of the excited state Γ_e, and the detuning of the two-photon transition δω. The two-photon operator is expressed in function of the scalar and the rank-two spherical tensors:

$$Q^S_{p_1 p_2} = \sum_{p=-2}^{2} \langle 11 p_1 p_2 | 2p \rangle Q_p^{(2)} + \langle 11 p_1 p_2 | 00 \rangle Q_0^{(0)} \tag{6}$$

Let's consider a two-photon transition between pure hyperfine levels $|g,J,J_z\rangle = |v,L,F,S,J,J_z\rangle$ and $|e,J',J'_z\rangle = |v',L',F',S',J',J'_z\rangle$ driven by electric fields with standard polarisations p_1 and p_2. If the ground state is not polarized, and in absence of a magnetic field, the two-photon transition probability at the two-photon resonance is calculated with the average contribution of the magnetic sublevels :

$$\begin{aligned} \overline{\Gamma}_{ge}^{(2)} &= \frac{4P_1 P_2}{\Gamma_e (S\hbar\varepsilon_0 c)^2} \frac{1}{2J+1} \\ &\times \sum_{k=0,2} \frac{\left| \langle g, J \| Q^{(k)} \| e, J' \rangle \right|^2}{2k+1} \left(\sum_p \left| \langle 11 p_1 p_2 | kp \rangle \right|^2 \right) \end{aligned} \tag{7}$$

where the reduced matrix elements of the two-photon operator are expressed as :

$$\begin{aligned} \langle g, J \| Q^{(k)} \| e, J' \rangle &= (-1)^{J'+L+k+S} \delta_{S,S'} \sqrt{(2J+1)(2J'+1)} \\ &\times \begin{Bmatrix} L' & J' & S \\ J & L & k \end{Bmatrix} \langle v, L \| Q^{(k)} \| v', L' \rangle \end{aligned} \tag{8}$$

The reduced matrix elements of the two-photon operator are expanded using the expression of the tensor product of dipole operators in function of the reduced matrix elements of the dipole operator with intermediate energy levels $|r\rangle = |v'',L'',F'',S'',J''\rangle$ and the detunings of the one-photon transitions from the ground level :

$$\frac{\langle v, L \| Q^{(k)} \| v', L' \rangle}{\sqrt{2k+1}} = (-1)^{k+2L+L'} \sqrt{(2L+1)(2L'+1)} \times \sum_{r(v'',L'')} \left[\begin{Bmatrix} 1 & 1 & k \\ L' & L & L'' \end{Bmatrix} \frac{\mu_{vL,v''L''} \mu_{v''L'',v'L'}}{\hbar(\omega - \omega_{gr})} \times (-1)^{L''} (2L''+1) \begin{pmatrix} L & 1 & L'' \\ 0 & 0 & 0 \end{pmatrix} \begin{pmatrix} L'' & 1 & L' \\ 0 & 0 & 0 \end{pmatrix} \right] \quad (9)$$

The two-photon matrix elements are calculated in this contribution for transitions of HD^+ in the terahertz or infrared domain that are far detuned comparing to the transitions in the UV or VUV domain to the excited electronic states. Therefore, intermediate energy levels from excited electronic states should bring to the two-photon operator matrix element a small contribution comparing to that given by Eq. (9). Table I shows the reduced matrix elements of the two-photon operator for the rotational transition and the rovibrational transition probed in the double resonance spectroscopy scheme. The calculations use the values of the HD^+ energy levels given in [26].

The matrix elements of the two-photon operator between the mixed hyperfine eigenvectors can be derived from Eq. (8) using the linear combinations of the pure hyperfine eigenvectors and the mixing coefficients. The selection rules for the two-photon transitions between pure hyperfine levels are $|L-L'|=0, \pm 2$, $|J-J'| \leq 2$ and $J_z - J'_z = -(p_1+p_2)$. Moreover, there is a strict selection rule on the total coupled spins $S'-S=0$ as the two-photon operator acts on the spatial part of the eigenvectors. Two-photon spin-forbidden transitions may be weakly allowed between mixed hyperfine levels due to the hyperfine couplings.

The matrix elements of the two-photon operator for the rotational and the rovibrational transition between mixed hyperfine structure energy levels are calculated using Eq. (7)–(9), the reduced matrix elements of the two-photon operators from Table I, the HD^+ ion energy levels from [26] and the mixing coefficients from the diagonalisation of the Hamiltonian. The mean squared matrix elements of the two-photon operator for standard $\pi\pi$ polarisations are shown in Figure 2 (a,b).

C. Discussion of systematic frequency shifts

For metrological applications, it is interesting to probe transitions with small Zeeman shifts, that were suggested in [18,27] :

- Transitions $\pi\pi$ between $J_z=0 \rightarrow J'_z=0$ states with quadratic Zeeman shift.

- Pairs of transitions $\sigma^+\sigma^-$ and $\sigma^-\sigma^+$ between pure hyperfine eigenvectors $|v,L,F=1,S=2,J=L+2,J_z=\pm(L+2)\rangle$ (stretched states). The Zeeman shifts of these transitions depend

linearly with the magnetic field, have the same magnitude but opposite values.

Selected transitions with small Zeeman shifts are shown in Table II. The Zeeman frequency shift coefficients are calculated using the dependences of HD^+ ion hyperfine energy levels on the magnetic field derived in [18]. Consider that the value of the magnetic field in the HD^+ ion trap is 20 mG. The Zeeman shifts for hyperfine components $J_z=0 \rightarrow J'_z=0$ of the two-photon rovibrational transition have absolute values less than 0.17 Hz, leading to accuracies from 3×10^{-16} to 3×10^{-15} (the uncertainty is conservatively estimated here as the value of the systematic shift). The hyperfine transition between the stretched states $(v,L,F,S,J,J_z)=(0,0,1,2,2,2) \rightarrow (2,0,1,2,2,2)$ has an extremely small linear Zeeman shift estimated at 0.2 mHz, leading to an accuracy of 3.6×10^{-18}. The hyperfine components with $J_z=0$ of the rotational transition display Zeeman shifts at the hertz level and accuracies from 2×10^{-13} to 3×10^{-12}. For comparison, for some two-photon hyperfine components $(v,L,F,S,J,J_z)=(0,0,F,S,J,J_z) \rightarrow (0,2,F,S,J+2,J_{z,2})$, the Zeeman shift coefficient is smaller than that of the corresponding hyperfine component $(v,L,F,S,J,J_z)=(0,0,F,S,J,J_z) \rightarrow (0,1,F,S,J+1,J_{z,1})$ of the one-photon transition. The two-photon transition between the stretched states has a Zeeman uncertainty four times smaller than the uncertainty of the corresponding one-photon transition. In the case of $J_z=0 \rightarrow J'_z=0$ transitions starting from the $(v,L,F,S,J,J_z)=(0,0,0,1,1,0)$ level, the use of two-photon spectroscopy provides an reduction of the Zeeman uncertainty by a factor of two.

The systematic effect may be reduced for the mean frequency of a pair of transitions that have linear Zeeeman shift coefficients with comparable absolute values but opposite signs, as proposed in [18,28]. The accuracy of the cancellation is estimated here for the rotational and the rovibrational transition at 3×10^{-16}.

The lightshift of the energy level $|n,J,J_z\rangle=|v,L,F,S,J,J_z\rangle$ for the interaction with counterpropagating beams with total intensity I (power in the standing-wave 2SI) is expressed as :

$$\delta E_n = -\frac{\alpha_n(\omega)}{2}\frac{I}{c} \tag{10}$$

The dynamic polarisability of an energy level can be calculated with the sum of contributions arising from transitions to other $1s\sigma_g$ rovibrational levels and to excited electronic states $\alpha_n(\omega)=\alpha_n^{rv}(\omega)+\alpha_n^{e}(\omega)$, as it was discussed in [29]. $\alpha_n(\omega)$ was calculated directly for several rovibrational levels of HD^+ ion using variational wavefunctions [17]. The rovibrational contribution to the dynamic polarisability is calculated here with the two-photon operator for pure hyperfine energy levels :

$$\alpha_n^{rv}(\omega) = -\left[\begin{array}{l}\langle n,J,J_z|Q^S_{\varepsilon\varepsilon^*}(E_n+\hbar\omega)|n,J,J_z\rangle \\ +\langle n,J,J_z|Q^S_{\varepsilon\varepsilon^*}(E_n-\hbar\omega)|n,J,J_z\rangle\end{array}\right]$$
$$\langle n,J,J_z|Q^S_{\varepsilon\varepsilon^*}(E_n\pm\hbar\omega)|n,J,J_z\rangle = \sum_{r,J'',J''_z}\frac{\langle n,J,J_z|D_{-p}|r,J'',J''_z\rangle\langle r,J'',J''_z|D_p|n,J,J_z\rangle}{E_n\pm\hbar\omega-E_r} \quad (11)$$

by taking into account the off-resonant couplings to the rovibrational energy levels in the $1s\sigma_g$ ground electronic state of HD^+ ion. The contributions to the dynamic polarisability arise from the scalar and the rank-two tensors, that are expressed as :

$$\langle v,L,F,S,J,J_z|Q_0^{(k)}(E_{vL}\pm\hbar\omega)|v,L,F,S,J,J_z\rangle = (-1)^{2J-J_z+L+k+S} \times\begin{pmatrix} J & k & J \\ -J_z & 0 & J_z\end{pmatrix}(2J+1)\begin{Bmatrix} L & J & S \\ J & L & k\end{Bmatrix}\langle v,L\|Q^{(k)}(E_{vL}\pm\hbar\omega)\|v,L\rangle \quad (12)$$

The reduced matrix element of the two-photon operator is expressed further in function of the reduced matrix elements of the dipole operator :

$$\frac{\langle v,L\|Q^{(k)}(E_{vL}\pm\hbar\omega)\|v,L\rangle}{\sqrt{2k+1}} = (-1)^{k+3L}(2L+1) \times\sum_{v'',L''}\left[\begin{array}{l}\begin{Bmatrix}1 & 1 & k \\ L & L & L''\end{Bmatrix}\frac{(-1)^{L''}(2L''+1)\mu^2_{vL,v''L''}}{(E_{vL}\pm\hbar\omega)-E_{v''L''}} \\ \times\begin{pmatrix}L & 1 & L'' \\ 0 & 0 & 0\end{pmatrix}\begin{pmatrix}L'' & 1 & L \\ 0 & 0 & 0\end{pmatrix}\end{array}\right] \quad (13)$$

As this contribution addresses transitions between low-lying rovibrational energy levels of the $1s\sigma_g$ electronic state that are in the terahertz and infrared domains, $\alpha_n^{rv}(\omega)$ values are calculated by taking into account off-resonant couplings up to the v=8 vibrational level. The transitions between these energy levels to excited electronic states are in the UV and VUV domains, therefore $\alpha_n^{e}(\omega)$ are neglected for the couplings driven by the THz-wave or the infrared laser. On the contrary, the cooling laser and the dissociation laser drive resonant couplings to the excited $2p\sigma_u$ state and the electronic contribution to the dynamic polarisability is dominant. In this case, $\alpha_n(\omega)$ for (v,L)=(0,0) are calculated directly from the frequency dependence derived in [17]. The dynamic polarisabilities for (v,L)=(0,2) and (v,L)=(2,0) are determined from the adjustment of some values for the v=0 and v=2 vibrational levels provided by [17] using a quadratic dependence

on the rotational quantum number $\alpha_{v,L}(\omega) = \alpha_{v,L=0}(\omega) + \delta\alpha_v(\omega) \times L(L+1)$. The hyperfine structure is not taken into account in the calculations of the dynamical polarisabilities in the UV domain. The lightshift parameters for selected hyperfine components of the two-photon rotational transition are derived subsequently and displayed in Table III. The lightshifts are estimated separately for interaction with a THz-wave with an intensity of 76.7 mW/cm^2, an infrared laser with an intensity of 38.7 W/cm^2, an HD^+ dissociation laser at 175 nm with an intensity of 6.1 W/cm^2, and an Be^+ cooling laser at 313 nm with an intensity of 0.8 mW/mm^2, respectively. These partial lightshifts are added to yield the total lightshift of each transition.

The lightshifts of the selected hyperfine components of the rovibrational transition induced by the infrared laser are -1.1 Hz, that corresponds to an accuracy of 1.9×10^{-14}. Probing in the same time the rotational transition is not required, although that has some advantages (see next section). The lighshifts induced by the THz-wave are comparable (-1.5 Hz for the transition between the stretched states) or significantly smaller (3.8 mHz for the transitions between J_z=0 levels). The lightshift induced by the dissociation laser is -0.1 Hz and the lightshift induced by the Be^+ cooling laser is -1.3 mHz.

The lightshifts of the hyperfine components with J_z=0 of the rotational transition induced by the THz-wave are from 11 mHz to 0.2 Hz. Moreover, the transition between the stretched states displays a lightshift of -2.4 mHz, that corresponds to 1.2×10^{-15} accuracy. Unfortunately, the REMPD detection scheme requires an infrared laser that induces lightshifts from -3.8 Hz to -4.3 Hz, for the transitions between J_z=0 levels, and -0.9 Hz for the transition between the stretched states, respectively. The lightshift induced by the dissociation laser is estimated at -1.5 mHz and the lightshift induced by the Be^+ cooling laser at -20 μHz. Cancellation of the total lightshift of the components of the rotational transition between hyperfine levels with J_z=0 can be achieved using an adjustment of the intensities of the THz-wave and the infrared laser, as suggested in [30]. The drawback of this approach is a possible reduction of the dissociation signal.

III. Double Resonance Two-Photon Spectroscopy

The proposed spectroscopy scheme with trapped HD^+ ions addresses conjointly the two-photon rotational transition (v,L)=(0,0)→(0,2) and the two-photon rovibrational transition (v,L)=(0,0)→(2,0). The detection is based on the photodissociation of the (v,L)=(2,0) level. The interaction with blackbody radiation recycles continuously population in the ground vibrational level. The change of the population in the rovibrational levels induced by the two-photon transitions is detected on the photodissociation signal. The intrinsic linewidths of the lasers and of

the THz-wave are assumed negligible. The hyperfine structure is not taken into account in this section.

The transition rate for the two-photon rovibrational transition is assumed at $\Gamma_{2ph,v} = 10\ s^{-1}$ that corresponds to a 5.36 μm infrared laser intensity estimated at 38.7 W/cm^2. The two-photon rotational transition rate is estimated at $\Gamma_{2ph,r}=2 \times 10^3\ s^{-1}$ for a THz-wave intensity of 76.7 mW/cm^2 that can be provided by a THz quantum cascade laser (QCL) emitting at 152.3 μm. Direct phase-locking of the THz QCL to the primary frequency standard is feasible using frequency multiplier technology based on Schottky diodes [31]. Dissociation of HD^+ ion from v=2 may be driven conveniently with radiation at 175 nm [32]. The dissociation rate assumed here at $\Gamma_{diss}=200\ s^{-1}$ may be reached with an intensity that is estimated at 6.1 W/cm^2. Obtaining such intensity may be feasible by frequency quadrupling of an amplified diode laser system at 700 nm and proper focusing of the 175 nm radiation or a sum frequency generation approach similar to [33]. A more practical alternative would be to exploit a high-power commercially available laser at 532 nm to dissociate HD^+ ions in higher rovibrational levels. Convenient REMPD schemes would involve, for example, excitation of (v,L)=(2,0)→(4,1) with an infrared laser at 2.95 μm and dissociation with the second harmonic at 266 nm, or excitation of (v,L)=(2,0)→(8,1) with an infrared laser at 1.11 μm and dissociation at 532 nm. The dissociation cross sections in these cases are similar with the value reached with 175 nm radiation [32]. The drawbacks of these alternatives are a possible reduction of the accuracies of the two-photon transitions by the lightshifts induced by the additional infrared laser. The trapped HD^+ ions are initially in the (v=0, L=0,…,5) levels with a population distribution determined by thermal equilibrium with blackbody radiation at 300 K. These levels are coupled with BBR-driven E1 rotational transitions. The transition rates from the higher (v',L') to the lower (v,L) level depend on the Einstein coefficients for the spontaneous emission $A_{vL}^{v'L'}$, the stimulated absorption $B_{v'L'}^{vL}$, and the stimulated emission $B_{vL}^{v'L'}$, respectively. Upon application of the THz-waves, the infrared and the dissociation lasers, the time dependences of the populations in different rovibrational levels $\rho_{v,L}(t)$ and in the dissociated state $\rho_{2p\sigma}(t)$ can be calculated with a set of rate equations depending on the two-photon transition rates given by Eq. (5) expressed with the values at resonance $\Gamma_{2ph,r,v}$ and the two-photon transition detunings $\delta\omega_{r,v}$:

$$
\begin{aligned}
&\frac{d\rho_{v=0,L}}{dt} = -\left(\begin{array}{l}\left(A^{v=0,L}_{v=0,L-1} + B^{v=0,L}_{v=0,L-1} W_T\left(\omega_{v=0;L,L-1}\right)\right)\times\left(1-\delta_{L,0}\right)\\ + B^{v=0,L}_{v=0,L+1} W_T\left(\omega_{v=0;L+1,L}\right)\end{array}\right)\rho_{v=0,L}\\
&+\left(A^{v=0,L+1}_{v=0,L} + B^{v=0,L+1}_{v=0,L} W_T\left(\omega_{v=0;L+1,L}\right)\right)\rho_{v=0,L+1}\\
&+ B^{v=0,L-1}_{v=0,L} W_T\left(\omega_{v=0;L,L-1}\right)\times\left(1-\delta_{L,0}\right)\rho_{v=0,L-1}\\
&+\delta_{v,0}\delta_{L,2}\frac{\Gamma_{2ph,r}\times\Gamma^2_{02}/4}{4\delta\omega_r^2+\Gamma^2_{02}/4}\left(\rho_{v=0,L=0}-\rho_{v=0,L=2}\right)\\
&-\delta_{v,0}\delta_{L,0}\left[\begin{array}{l}\frac{\Gamma_{2ph,r}\times\Gamma^2_{02}/4}{4\delta\omega_r^2+\Gamma^2_{02}/4}\left(\rho_{v=0,L=0}-\rho_{v=0,L=2}\right)\\ \frac{\Gamma_{2ph,v}\times\Gamma^2_{20}/4}{4\delta\omega_v^2+\Gamma^2_{20}/4}\left(\rho_{v=0,L=0}-\rho_{v=2,L=0}\right)\end{array}\right];\\
&\frac{d\rho_{v=2,L=0}}{dt} = \frac{\Gamma_{2ph,v}\times\Gamma^2_{20}/4}{4\delta\omega_v^2+\Gamma^2_{20}/4}\left(\rho_{v=0,L=0}-\rho_{v=0,L=2}\right)\\
&-\left(\Gamma_{diss}+\Gamma_{20}\right)\rho_{v=2,L=0};\\
&\frac{d\rho_{2p\sigma}}{dt} = \Gamma_{diss}\rho_{v=2,L=0}
\end{aligned}
\qquad (14)
$$

The spectral energy of the blackbody radiation at temperature T at the angular frequency of a rotational transition is denoted $W_T(\omega)$. Transition rates to excited rovibrational and electronic levels are assumed fast enough to neglect spontaneous decay to lower energy levels. The calculations use the radiative linewidths $\Gamma_{02,20}$ derived from the lifetimes of the HD^+ rovibrational levels given in [34]. The rate equations are numerically integrated, by assuming $\Sigma_{v,L}\rho_{v,L}(t)+\rho_{2p\sigma}(t)=1$. The dependence of the photodissociated fraction on the two-photon rotational detuning, when the infrared laser is tuned at the two-photon rovibrational resonance, is shown in Figure 3(a). The lineshape is well adjusted by a Lorentzian with 447 mHz full width at half maximum (FWHM) linewidth. The rotational spectrum is superposed on a small flat baseline determined by the rovibrational excitation. The resolution is 2.3×10^{-13}, that improves by three orders of magnitude the resolution predicted for two-photon rovibrational spectroscopy of trapped HD^+ in the Lamb-Dicke regime [11]. The dependence of the photodissociated fraction in function of the two-photon rovibrational detuning with or without coupling on the two-photon rotational resonance is displayed in Figure 3(b). The lineshapes are well adjusted by Lorentzians with full width at half maximum (FWHM) linewidths of 12.1 Hz and 20.0 Hz, respectively. Probing the rovibrational transition conjointly with the rotational transition is not required in this detection scheme but allows signal narrowing and enhancement.

The contrast of the two-photon rotational line is defined as $C=(\rho_{2p\sigma,res}-\rho_{2p\sigma,0})/\rho_{2p\sigma,0}$ in function of the photodissociated fraction at two-photon rotational and rovibrational resonances $\rho_{2p\sigma,res}$ and the baseline due to the rovibrational excitation $\rho_{2p\sigma,0}$. The dependence of the contrast on the two-photon rotational transition rate is shown on Figure 4, left-axis. Here, the THz-wave and the

infrared laser are tuned at the two-photon rotational and rovibrational resonances. For the same transition rates, the contrast is enhanced by an order of magnitude comparing to the contrast obtained in the spectroscopy scheme based on the (v,L)=(0,1)→(0,3) and (v,L)=(0,3)→(9,3) transitions [12]. As shown on Figure 4, right-axis, reduction of the transition rate allows to decrease the linewidth of the rotational line by an order of magnitude to a few tens of mHz by maintaining the same contrast. The rate equation model does not take into account coherence effects and ion motion in the trap. A more accurate lineshape may be derived by using the density matrix representation and by solving the optical Bloch equations in the multilevel system [11]. That will allow to describe conjointly the effects of micromotion, power broadening, photodissociation and interaction with the BBR and may lead to broader lines than those calculated with the rate equation model.

IV. Determination of Fundamental Constants

The comparison between *ab-initio* calculations and experimental frequencies of two-photon rotational and rovibrational HMI transitions, following the approach of CODATA least-squares adjustment [14], may provide a determination of fundamental constants. There are two requirements for doing this comparison. First, the theory should characterize correctly the molecular system and the experimental frequencies should not be altered by the measurement procedure. Second, the theoretical prediction and the experimental data should agree within their uncertainties. As a general rule, if the frequency uncertainty is the same, an increase of the number of transitions used in the comparison may improve the determination of fundamental constants.

Quantum electrodynamics allows to express the energy levels of HD^+ ions as a series expansion :

$$E = R_\infty \left[\begin{array}{l} E_{nr}(\mu_{pe}, \mu_{dp}) + \alpha^2 F_{QED}(\alpha, \mu_{pe}, \mu_{dp}) \\ + \left(A_p^{fs} (r_p / a_0)^2 + A_d^{fs} (r_d / a_0)^2 \right) \end{array} \right] \quad (15)$$

that depends on the Rydberg constant R_∞, the proton-to-electron mass ratio $\mu_{pe} = M_p/m_e$, the deuteron-to-proton mass ratio $\mu_{dp} = M_d/M_p$, the fine-structure constant α, the proton radius r_p, the deuteron radius r_d, and the Bohr radius $a_0 = \alpha/4\pi R_\infty$. The first term corresponds to the nonrelativistic energy, the next term to a series expansion of corrections that are ordered in function of the QED parameter α, the relativistic parameter $Z_{p,d}\alpha$ expressed with the nuclear

charge $Z_{p,d}$, and the recoil parameter $m_e/M_{p,d}$. The last terms, depending on the Bohr radius, are associated to the finite-size of the proton and the deuteron. Energy levels of H_2^+ may be expressed in a similar way in function on R_∞, μ_{pe} and r_p.

The sensitivity coefficient of a transition frequency f to a constant c is :

$$K_c = \frac{c_0}{f_0}\left(\frac{df}{dc}\right)_{c_0} \tag{16}$$

Here, the frequency f_0 is calculated with the set of the recommended values of fundamental constants $\{c_0\}$ given by CODATA. Table IV shows the sensitivity coefficients for selected two-photon HMI transitions which are calculated here using the dependences on fundamental constants of different terms in Eq. (15). The sensitivity coefficients to μ_{pe} and μ_{dp} are derived using non-relativistic calculations of $\partial E/\partial \ln(\mu_{pe,dp})$ from [35,36]. The recoil corrections have negligible contributions to these sensitivity coefficients. Sensitivity to α is not addressed in this contribution and the sensitivity coefficients to R_∞ are assumed equal to 1. The sensitivity coefficients to r_p and r_d are derived using finite-size correction parameters from [2]. The calculated values of the sensitivity coefficients for transitions N° 1-9 agree with the results of [37].

The uncertainty of the determination of fundamental constants depends on the accuracy of the experimental frequencies and the accuracy of the theoretical calculations. The accuracy of HMI spectra can be estimated by considering the signal-to-noise ratio obtained in actual experimental setups and the expected linewidth for two-photon spectroscopy. The rovibrational lines may be measured with an accuracy of 10^{-12} [9]. The accuracy of the rotational lines is assumed at 5×10^{-13}. The theoretical calculations may reach an accuracy estimated at 3×10^{-12} [37].

The dependence of the transition frequencies on the constants is linearized and expressed in a matrix form Y = AX, where $Y = \{y_1, y_2, \ldots, y_{N1}\}$ is a column of N_1 elements $y_i = (f_i - f_{i,0})/f_{i,0}$, and $X = \{x_1, x_2, \ldots, x_{N2}\}$ is a column with N_2 elements $x_j = (c_j - c_{j,0})/c_{j,0}$,. A is the sensitivity matrix of size $N_1 \times N_2$ with elements $a_{ij} = d(\ln f_{0,i})/d(\ln c_{0,j})$. The covariance matrix G of the solution $\hat{X}$ is expressed in terms of the covariance matrix of the input data V and the sensitivity matrix as :

$$G = \left(A^T V^{-1} A\right)^{-1} \tag{17}$$

The covariance matrix of the input data V is constructed as follows : the uncertainty is the root-

mean-square sum of the experimental and theoretical uncertainties and the covariances are given by the covariances of the predictions. It is assumed that the experimental frequencies are not correlated and the correlation coefficients of the predictions are equal to 1. Non-zero covariance arises from the uncalculated terms in the energy levels that are expressed as a particular constant multiplied by the common factor arising, for example, from the overlapping of the electron wavefunction with the extended nuclear charge distribution. The use of the relative values and of the sensitivity coefficients has the advantage to provide a simple expression for the solution in the linear approximation :

$$\hat{X} = GA^T V^{-1} Y \tag{18}$$

The uncertainties of the determination of fundamental constants are calculated for different combinations of H_2^+ and HD^+ transitions. The values of R_∞, μ_{pe}, μ_{dp}, r_p, r_d may be derived from an adjustment of transitions N° 1-8 shown in Table IV. The results are displayed in Table V on the first line. This adjustment provides a way to improve the accuracy of μ_{pe} by an order of magnitude and the accuracy of μ_{dp} by a factor of 20, comparing to the relevant values from CODATA 2014 [14]. The accuracies for the determination of R_∞, r_p, r_d are comparable with the corresponding CODATA 2014 values. This approach yields a determination of fundamental constants that is independent on previous results. As the uncertainties of the determination of proton and deuteron radii are smaller than the known discrepancies [38], this approach may provide a new insight into the proton radius puzzle.

An accurate determination of r_p and r_d may be provided by muonic hydrogen and muonic deuterium spectroscopy. If the proton radius puzzle is solved, one can use atomic spectroscopy values for r_p, r_d in the adjustments of HMI transitions. For example, the adjustment of 4 transitions (second line in Table V) allows determination of three constants (R_∞, μ_{pe}, μ_{dp}). The accuracies are improved by factors of (2, 79, 44) compared to the relevant CODATA 2014 values. Finally, if R_∞, r_p, r_d are determined accurately in atomic spectroscopy, the adjustment of three transitions, shown on the third line of Table V, yields values of μ_{pe} and μ_{dp} with accuracies improved by factors of (68, 42) compared to the relevant values provided by CODATA 2014. Note that the use of two two-photon rotational lines and a two-photon rovibrational line in the adjustment improves the accuracy for μ_{pe} and μ_{dp} by a factor of 5 comparing to a previous result that uses two two-photon rovibrational lines [37]. Adding rotational transitions to the adjustment is advantageous for improving the determination of fundamental constants because their

sensitivity coefficients are by two times higher than the relevant sensitivity coefficients of the rovibrational transitions.

V. CONCLUSION

A double resonance two-photon spectroscopy scheme with trapped and sympathetically cooled hydrogen molecular ions is exploited for a determination of fundamental constants. This contribution discusses the detection by photodissociation of a two-photon rotational transition and a two-photon rovibrational transition on cold trapped HD^+ ions. The two-photon lineshapes are calculated using a rate equation model for HD^+ ions populations. The spectroscopy scheme provides a resolution at the 10^{-13} level. The proposed experimental approach uses equal-frequency counterpropagating THz and infrared waves for probing HD^+ transitions, a HD^+ dissociation laser at 175 nm and a 313 nm Be^+ ion cooling laser, that shift the frequencies of the two-photon transitions due to the AC-Stark effect by an amount that is carefully estimated. The lightshifts for selected hyperfine components of the rovibrational transition are at the 10^{-14} level. The lightshifts for the hyperfine components of the rotational transition, estimated at the 10^{-12} level, are imposed by off-resonant couplings of the infrared radiation used in the REMPD detection scheme. The Zeeman shifts are in the range from the 10^{-18} to 10^{-15} level for selected hyperfine components of the rovibrational transition, and from the 10^{-13} to 10^{-12} level for selected hyperfine components of the rotational transition.

The experimental accuracy with two-photon transitions of hydrogen molecular ions is estimated with signal-to-noise ratio and linewidth considerations at the 10^{-12} level, which corresponds also to the level of accuracy of *ab-initio* energy level calculations. The comparison of experimental data and theoretical calculations may provide an independent and accurate determination of the Rydberg constant, the proton-to-electron mass ratio and the deuteron-to-proton mass ratio, respectively. It allows a determination of the proton and deuteron radii by molecular spectroscopy. Depending on possible issues of the proton radius puzzle, the two-photon spectroscopy of hydrogen molecular ions may lead to an improvement of the determination of the proton-to-electron mass ratio and deuteron-to-proton mass ratio at the 10^{-12} level.

ACKNOWLEDGMENT

The author acknowledges support for this work from the University Lille 1 and the CNRS.

REFERENCES

[1] V.I. Korobov, "Bethe logarithm for the hydrogen molecular ion HD^+," Phys. Rev. A, vol. 70, pp. 012505, July 2004.

[2] V.I. Korobov, "Leading-order relativistic and radiative corrections to the rovibrational spectrum of H_2^+ and HD^+," Phys. Rev. A, vol. 74, pp. 052506, November 2006.

[3] V.I. Korobov, "Relativistic corrections of $m\alpha^6$ order to the rovibrational spectrum of H_2^+ and HD^+ molecular ions," Phys. Rev. A, vol. 77, pp. 022509, February 2008.

[4] V.I. Korobov, L. Hilico, and J.-Ph. Karr, "Theoretical transition frequencies beyond 0.1 p.p.b. accuracy in H_2^+, HD^+, and antiprotonic helium," Phys. Rev. A, vol. 89, pp. 032511, March 2014.

[5] V.I. Korobov, L. Hilico, and J.-Ph. Karr, "$m\alpha^7$-Order corrections in the hydrogen molecular ions and antiprotonic helium," Phys. Rev. Lett., vol. 112, pp. 103003, March 2014.

[6] V.I. Korobov, L. Hilico, and J.-Ph. Karr, "Fundamental transitions and ionization energies of the hydrogen molecular ions with few ppt uncertainty," Phys. Rev. Lett., vol. 118, pp. 233001, June 2017.

[7] J.C.J. Koelemeij, B. Roth, A. Wicht, I. Ernsting, and S. Schiller, "Vibrational spectroscopy of HD^+ with 2-ppb accuracy," Phys. Rev. Lett., vol. 98, pp. 173002, April 2007.

[8] U. Bressel, A. Borodin, J. Shen, M. Hansen, I. Ernsting, and S. Schiller, "Manipulation of individual hyperfine states in cold trapped molecular ions and application to HD^+ frequency metrology," Phys. Rev. Lett., vol. 108, pp. 183003, May 2012.

[9] J. Biesheuvel, J.-Ph. Karr, L. Hilico, K.S.E. Eikema, W. Ubachs, and J.C.J. Koelemeij, "Probing QED and fundamental constants through laser spectroscopy of vibrational transitions in HD^+," Nat. Commun., vol. 7, pp. 10385, January 2016.

[10] E.J. Salumbides, J.C.J. Koelemeij, J. Komasa, K. Pachucki, K.S.E. Eikema, and W. Ubachs, "Bounds on fifth forces from precision measurements on molecules," Phys. Rev. D, vol. 87, pp. 112008, June 2013.

[11] V.Q. Tran, J.-Ph. Karr, A. Douillet, J.C.J. Koelemeij, and L. Hilico, "Two-photon spectroscopy of trapped HD^+ ions in the Lamb-Dicke regime," Phys. Rev. A, vol. 88, pp. 033421, September 2013.

[12] F.L. Constantin, "THz/infrared double resonance two-photon spectroscopy of HD^+ for determination of fundamental constants," Atoms, vol. 5, pp. 38, October 2017.

[13]S. Alighanbari, M. Hansen, V.I. Korobov, and S. Schiller, ”Rotational spectroscopy of cold and trapped molecular ions in the Lamb-Dicke regime,” Nat. Phys., vol. 14, pp. 555−559, March 2018.

[14]P.J. Mohr, B. Taylor, and D.B. Newell, “CODATA recommended values of the fundamental physical constants: 2014,” Rev. Mod. Phys., vol. 88, pp. 035009, September 2016.

[15]S. Patra, J.-Ph. Karr, L. Hilico, M. Germann, V.I. Korobov, and J.C.J. Koelemeij, “Proton–electron mass ratio from HD^+ revisited,” J. Phys. B, vol. 51, pp. 024003, December 2017.

[16]F.L. Constantin, “Double resonance two-photon interrogations of hydrogen molecular ions for determination of fundamental constants,” in *Proc. CPEM*, Paris, France, 2018, pp. 8501094.

[17]S. Schiller, D. Bakalov, A.K. Bekbaev, and V.I. Korobov, “Static and dynamic polarizability and the Stark and blackbody-radiation frequency shifts of the molecular hydrogen ions H_2^+, HD^+, and D_2^+,” Phys. Rev. A, vol. 89, pp. 052521, May 2014.

[18]D. Bakalov, V.I. Korobov, and S. Schiller, “Magnetic field effects in the transitions of the HD^+ molecular ion and precision spectroscopy,” J. Phys. B, vol. 44, pp. 025003, January 2011.

[19]D. Bakalov, V.I. Korobov, and S. Schiller, “High-precision calculation of the hyperfine structure of the HD^+ ion,” Phys. Rev. Lett., vol. 97, pp. 243001, December 2006.

[20]J. Ph. Karr, S. Kilic, and L. Hilico, “Energy levels and two-photon transition probabilities in the HD^+ ion,” J. Phys. B, vol. 38, pp. 853−866, March 2005.

[21]B. Cagnac, G. Grynberg, and F. Biraben, “Spectroscopie d’absorption multiphotonique sans effet Doppler,” J. Phys. France, vol. 34, pp. 845–858, Octobre 1973.

[22]C.A. Leach and R.E. Moss, “Spectroscopy and quantum mechanics of the hydrogen molecular cation : A test of the molecular quantum mechanics,” Annu. Rev. Phys. Chem., vol. 46, pp. 55–82, October 1995.

[23]A. Carrington, I.R. McNab, and C.A. Montgomerie, “Spectroscopy of the hydrogen molecular ion,” J. Phys. B, vol. 22, pp. 3551–3586, November 1989.

[24]J. Brown and A. Carrington, Rotational Spectroscopy of Diatomic Molecules, 1st ed, Cambridge: Cambridge University Press, 2003.

[25]D. Bakalov and S. Schiller, “Static Stark effect in the molecular ion HD^+,” Hyperfine Interact., vol. 210, pp. 25–31, May 2012.

[26]R.E. Moss, “Calculations for vibration-rotation levels of HD^+, in particular for high N,” Mol. Phys., vol. 78, pp. 371−405, 1993.

[27]D. Bakalov and S. Schiller, “The electric quadrupole moment of molecular hydrogen ions and their potential for a molecular ion clock,” Appl. Phys. B, vol. 114, pp. 213–230, January 2014.

[28]S. Schiller, D. Bakalov, and V.I. Korobov, “Simplest molecules as candidates for precise optical clocks,” Phys. Rev. Lett., vol. 113, pp. 023004, July 2014.

[29]J.C.J. Koelemeij, “Infrared dynamic polarizability of HD^+ rovibrational states,” Phys. Chem. Chem. Phys., vol. 13, pp. 18844–18851, November 2011.

[30]F.L. Constantin, “Two-photon spectroscopy of hydrogen molecular ions for precision measurements of fundamental constants,” in *Proc. EFTF*, Torino, Italy, 2018, pp. 330−337.

[31]A. Danylov, N. Erickson, A. Light, and J. Waldman, “Phase locking of 2.324 and 2.959 terahertz quantum cascade lasers using a Schottky diode harmonic mixer,” Opt. Lett., vol. 40, pp. 5090−5092, November 2015.

[32] M. Tajeddine and G. Parlant, “Computed photodissociation cross sections of HD^+ and Franck-Condon factors for the ionization of HD,” Mol. Phys., vol. 33, pp. 1797−1803, 1977.

[33]S. Galtier, F. Nez, L. Julien, F. Biraben, “Ultraviolet continuous-wave laser source at 205 nm for hydrogen spectroscopy,” Opt. Comm., vol. 324, pp. 34−37, August 2014.

[34]Z. Amitay, D. Zajfman, and P. Forck, “Rotational and vibrational lifetime of isotopically asymmetrized homonuclear diatomic molecular ions,” Phys. Rev. A, vol. 50, pp. 2304–2308, September 1994.

[35]S. Schiller and V. Korobov, “Tests of time independence of the electron and nuclear masses with ultracold molecules,” Phys. Rev. A, vol. 71, pp. 032505, March 2005.

[36]J. Ph. Karr and L. Hilico, “High accuracy results for the energy levels of the molecular ions H_2^+ , D_2^+ and HD^+, up to J = 2,” J. Phys. B, vol. 39, pp. 2095–2105, April 2006.

[37]J.-Ph. Karr, L. Hilico, J.C.J. Koelemeij, and V.I. Korobov, “Hydrogen molecular ions for improved determination of fundamental constants,” Phys. Rev. A, vol. 94, pp. 050501, November 2016.

[38]R. Pohl et al., “Deuteron charge radius and Rydberg constant from spectroscopy data in atomic deuterium,” Metrologia, vol. 54, pp. L1–L10, March 2017.

Figure captions

Fig. 1. Hyperfine structure of the HD^+ ion energy levels. The values of the hyperfine-free rovibrational energies are subtracted.

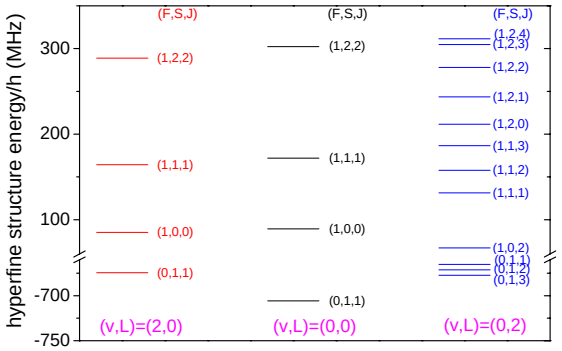

Fig. 2. Average of the squared two-photon reduced matrix elements, in atomic units, for the hyperfine components of (a): the rovibrational transition (v,L)=(0,0)→(2,0), and (b): the rotational transition (v,L)=(0,0)→(0,2), respectively. Excitation with π–polarized counterpropagating waves. The spectra are centered on the hyperfine-free frequencies from Table I.

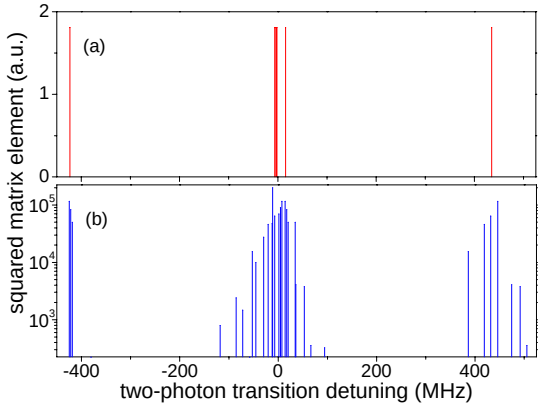

Fig. 3. (a) Spectrum of the two-photon rotational transition (magenta line) at the two-photon rovibrational resonance. (b) Spectra of the two-photon rovibrational transition calculated with (red line) and without (blue line) the THz-wave tuned at the two-photon rotational resonance. FWHM linewidths are shown on the plots. Parameters used for calculations $\Gamma_{2ph,r}$=2000 s^{-1}, $\Gamma_{2ph,v}$=10 s^{-1}, Γ_{diss}=200 s^{-1}, REMPD time 10 s.

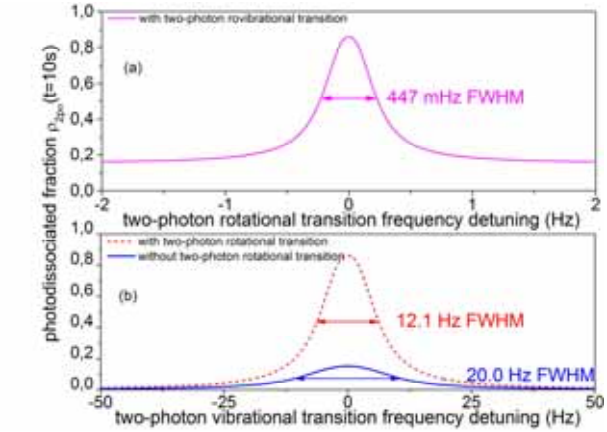

Fig. 4. Dependence of the contrast of the two-photon rotational line on the two-photon rotational transition rate (black circles, left-axis). Dependence of the FWHM linewidth of the two-photon rotational line on the two-photon rotational transition rate (red triangles right-axis). Parameters used for calculations $\Gamma_{2ph,v}$=10 s^{-1}, Γ_{diss}=200 s^{-1}, REMPD time 1 s.

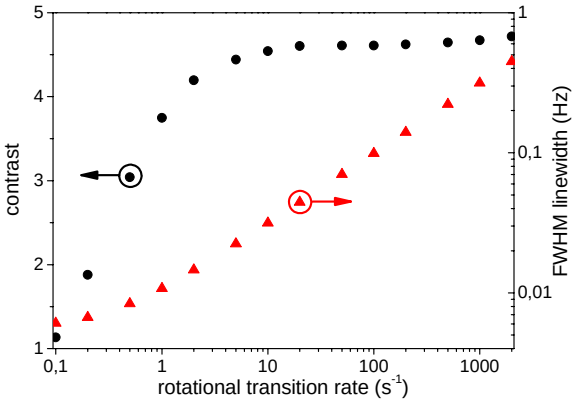

Table captions

Table I: Reduced matrix elements of the two-photon operator for the transitions (v,L)→(v',L') in atomic units.

v	L	v'	L'	Frequency (THz)	$Q^{(2)}_{vL;v'L'}$ (a.u.)	$Q^{(0)}_{vL;v'L'}$ (a.u.)
0	0	0	2	1.968	1367.669	0
0	0	2	0	55.909	0	2.329

Table II: Zeeman shift coefficients for selected hyperfine components of the two-photon rotational and rovibrational transitions. (a) transitions between J_z=0 states. (b) transitions between stretched states.

(a)		
$v,L,F,S,J;J_z$	$v',L',F',S',J';J'_z$	$\Delta\eta_{B^2}$ (Hz/G^2)
0,0,0,1,1;0	0,2,0,1,3;0	-1062.0
0,0,1,0,0;0	0,2,1,0,2;0	3100.0
0,0,1,1,1;0	0,2,1,1,3;0	-3786.0
0,0,1,2,2;0	0,2,1,2,4;0	16084.5
0,0,0,1,1;0	2,0,0,1,1;0	-48.0
0,0,1,0,0;0	2,0,1,0,0;0	-409.0
0,0,1,1,1;0	2,0,1,1,1;0	342.0
0,0,1,2,2;0	2,0,1,2,2;0	114.5
(b)		
$v,L,F,S,J;J_z$	$v',L',F',S',J';J'_z$	$\Delta\eta_B$ (Hz/G)
0,0,1,2,2;2	0,2,1,2,4;4	-555.9
0,0,1,2,2;2	2,0,1,2,2;2	0.01

TABLE III: Lightshift coefficients for hyperfine components induced by radiation tuned at the hyperfine-free frequency of a two-photon transition $(v_1,L_1)\rightarrow(v_2,L_2)$, by the dissociation laser, and by the cooling laser, respectively. The coupling is with radiation with standard polarisations p_1, p_2.

$v,L,F,S,J;J_z$	$v',L',F',S',J';J'_z$	v_1	L_1	v_2	L_2	p_1	p_2	$\Delta\eta_{LS}$ (Hzcm^2/W)
0,0,0,1,1;0	0,2,0,1,3;0	0	0	0	2	0	0	1.374
0,0,1,0,0;0	0,2,1,0,2;0	0	0	0	2	0	0	0.110
0,0,1,1,1;0	0,2,1,1,3;0	0	0	0	2	0	0	1.374
0,0,1,2,2;0	0,2,1,2,4;0	0	0	0	2	0	0	1.916
0,0,1,2,2;2	0,2,1,2,4;4	0	0	0	2	1	-1	-3.271
0,0,0,1,1;0	0,2,0,1,3;0	0	0	2	0	0	0	-0.103
0,0,1,0,0;0	0,2,1,0,2;0	0	0	2	0	0	0	-0.112
0,0,1,1,1;0	0,2,1,1,3;0	0	0	2	0	0	0	-0.103
0,0,1,2,2;0	0,2,1,2,4;0	0	0	2	0	0	0	-0.099
0,0,1,2,2;2	0,2,1,2,4;4	0	0	2	0	1	-1	-0.090
$(v,L)=(0,0)$	$(v,L)=(0,2)$	175 nm				0		-2.54×10^{-4}
$(v,L)=(0,0)$	$(v,L)=(0,2)$	313 nm				0		-2.51×10^{-4}
$0,0,F,S,J;0$	$2,0,F',S',J';0$	0	0	0	2	0	0	7.401
$0,0,F,S,J;0$	$2,0,F',S',J';0$	0	0	2	0	0	0	-1.74×10^{-2}
0,0,1,2,2;2	2,0,1,2,2;2	0	0	0	2	1	-1	-3.80×10^{-2}
0,0,1,2,2;2	2,0,1,2,2;2	0	0	2	0	1	-1	2.81×10^{-2}
$(v,L)=(0,0)$	$(v,L)=(2,0)$	175 nm				0		-1.66×10^{-2}
$(v,L)=(0,0)$	$(v,L)=(2,0)$	313 nm				0		-1.61×10^{-2}

TABLE IV: Sensitivity coefficients to constants for two-photon transitions of HD^+ (lines n° 1-4,9) and H_2^+ (lines n° 5-8,10).

$N°$	v	L	v'	L'	$K_{\mu pe}$	$K_{\mu dp}$	$10^9 \times K_{rp}$	$10^9 \times K_{rd}$
1	0	0	0	2	-0.9848	-0.3284	-1.0581	-6.3355
2	0	1	0	3	-0.9808	-0.3271	-1.0547	-6.3151
3	0	1	2	1	-0.4601	-0.1534	-0.6192	-3.7012
4	0	3	9	3	-0.3522	-0.1175	-0.5880	-3.5000
5	0	2	1	2	-0.4657	0	-1.2400	0
6	3	2	4	2	-0.3652	0	-1.1730	0
7	5	2	6	2	-0.2801	0	-1.1330	0
8	6	2	7	2	-0.2279	0	-1.1140	0
9	0	0	2	0	-0.4612	-0.1538	-0.6200	-3.7054
10	0	0	0	2	-0.9819	0	-2.1123	0

TABLE V: Uncertainties for determination of fundamental constants with adjustments of two-photon transitions of hydrogen molecular ions from Table IV.

$N°$ transition in adjustment	$\Delta x(R_\infty)$ $\times 10^{11}$	$\Delta x(\mu_{pe})$ $\times 10^{11}$	$\Delta x(\mu_{dp})$ $\times 10^{11}$	$\Delta x(r_p)$ $\times 10^3$	$\Delta x(r_d)$ $\times 10^3$
1,2,3,4,5,6,7,8	0.84	0.78	0.55	8.2	3.3
1,4,8,10	0.31	0.12	0.21		
1,8,10		0.14	0.22		